Supplementary Information (SI) for Journal of Materials Chemistry C.

Sensitivity Augmentation in Multimodal Optical Thermometry based on $NaBi(MoO_4)_2:Yb^{3+}$, Er^{3+}@$NaBi(MoO_4)_2:Yb^{3+}$, Ho^{3+} core@shell nanoparticles

Satish Kumar Samal[†], Nishanth Dominic[†], Jyoti Yadav[†], Sahana Kulkarni[†], Srungarpu N. Achary[§] and Boddu S. Naidu[†,*]

[†]*Energy and Environment Unit, Institute of Nanoscience and Technology (INST), Mohali, Punjab, India-140306.*

[§]*Chemistry Division, Bhabha Atomic Research Centre, Trombay, Mumbai 140085, India*

*E-mail address: naidu245@gmail.com, sanyasinaidu@inst.ac.in

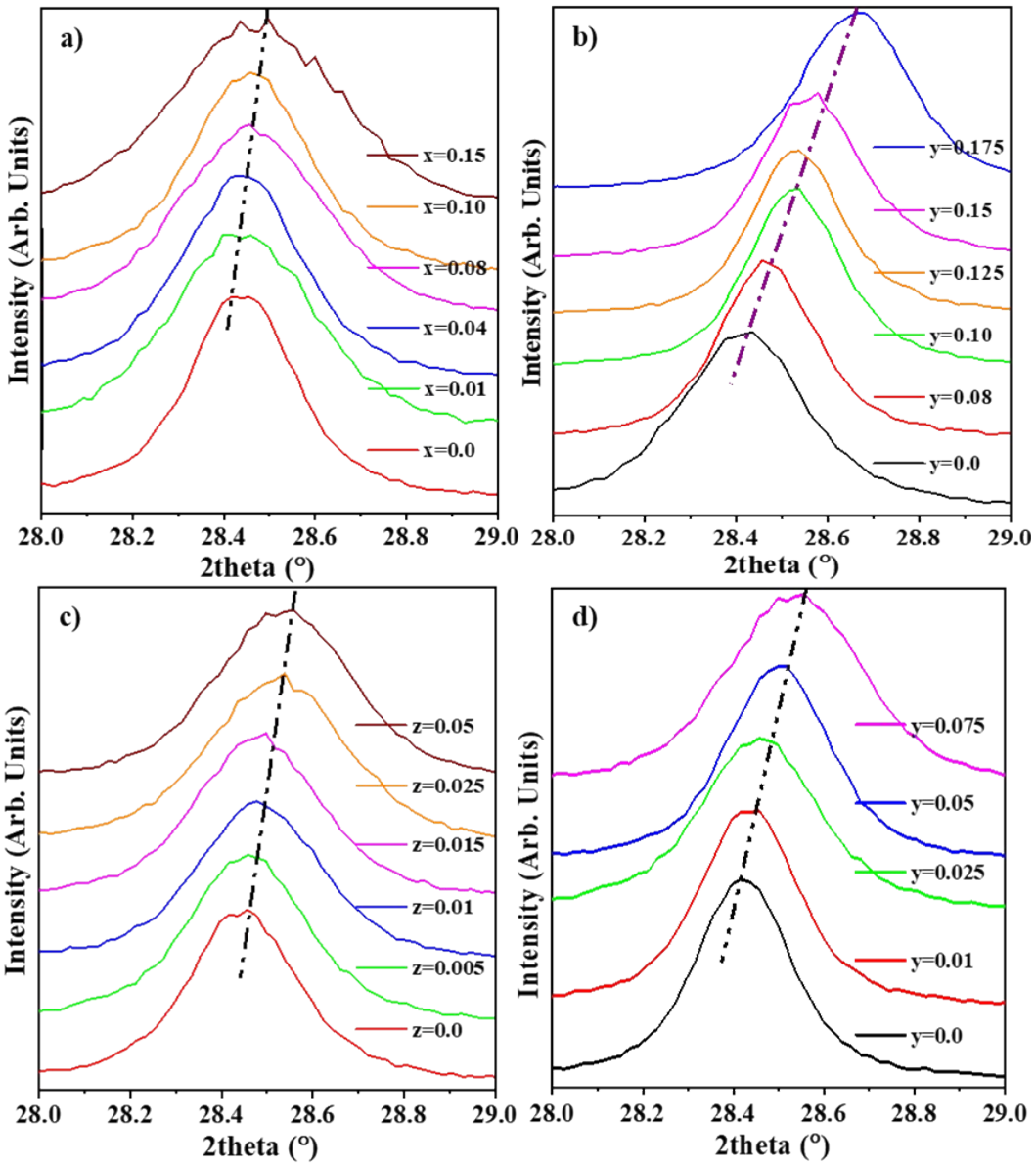

Fig. S1. Magnified view of the intense (112) reflection in XRD patterns of (a) NBM: x Er^{3+}, (b) NBM: y Yb^{3+}, 0.08 Er^{3+}, (c) NBM: 0.05 Yb^{3+}, z Ho^{3+} and (d) NBM: y Yb^{3+}, 0.01 Ho^{3+}.

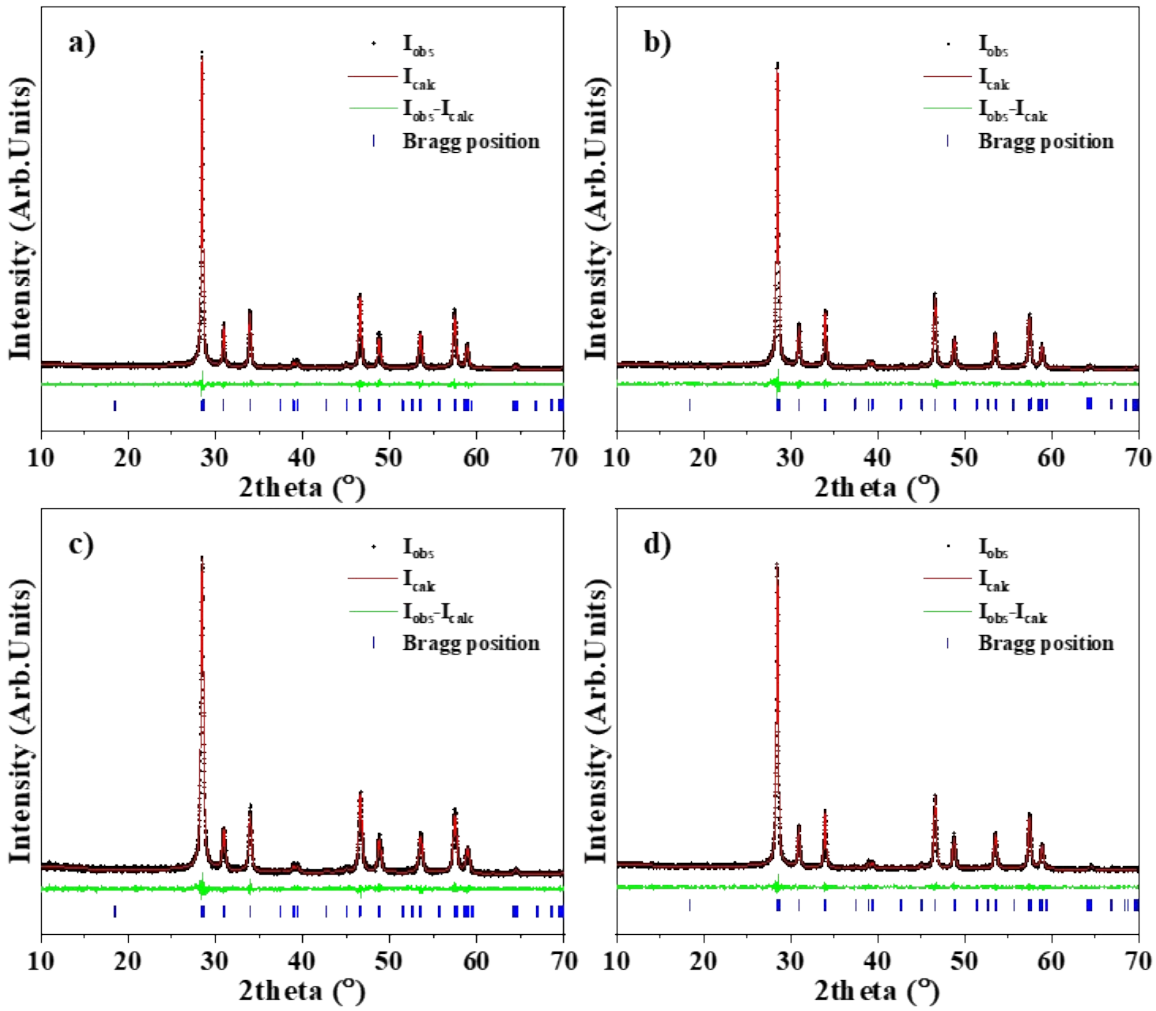

Fig. S2. Rietveld refinement plot of the powder XRD data of (a) $NaBi(MoO_4)_2$:0.01Yb^{3+}, 0.01Ho^{3+}, (b) $NaBi(MoO_4)_2$:0.025Yb^{3+}, 0.01Ho^{3+}, (c) $NaBi(MoO_4)_2$:0.05Yb^{3+}, 0.01Ho^{3+}, and (d) $NaBi(MoO_4)_2$:0.075Yb^{3+}, 0.01Ho^{3+}.

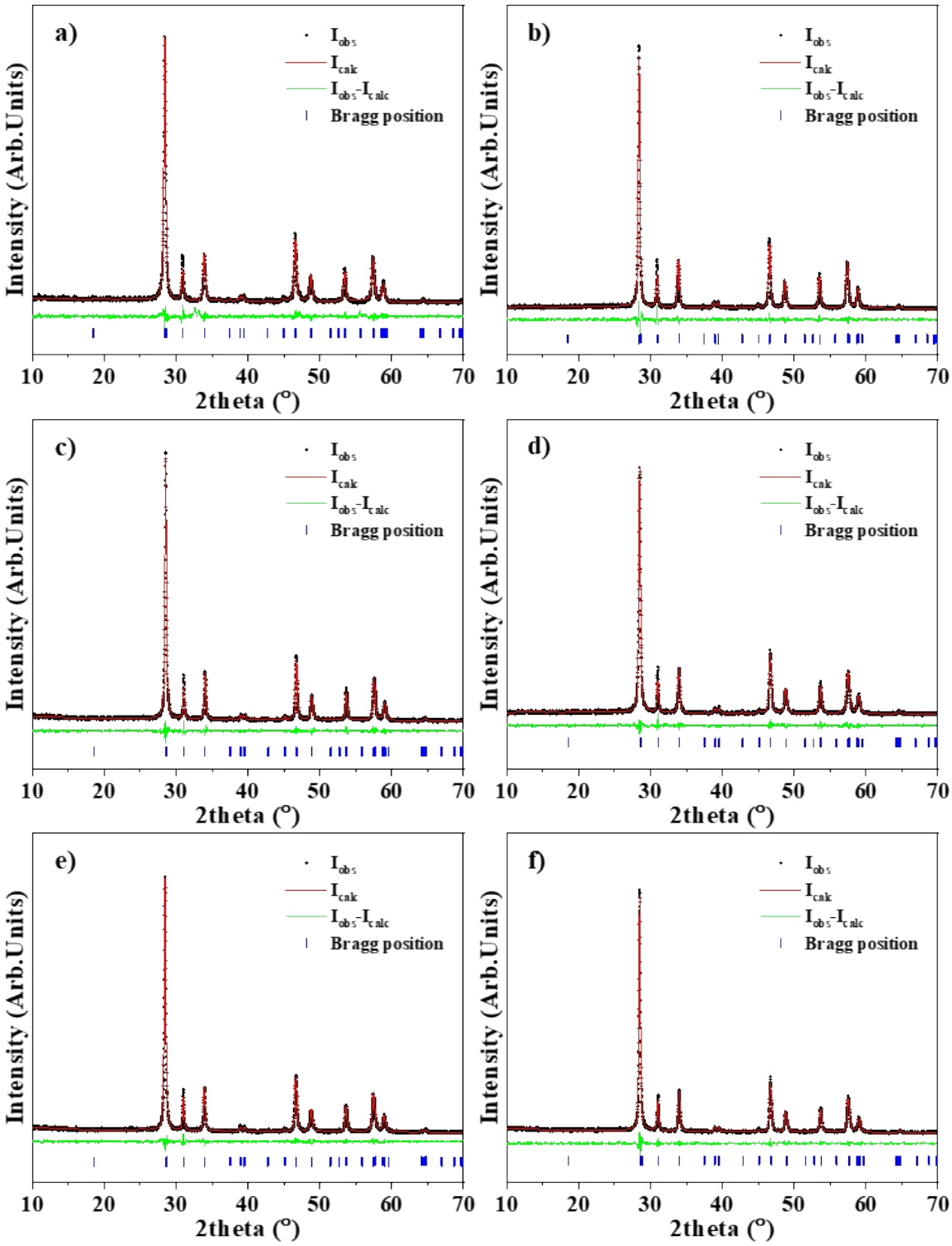

Fig. S3. Rietveld refinement plot of the powder XRD data of (a) $NaBi(MoO_4)_2$:$0.08Er^{3+}$, (b) $NaBi(MoO_4)_2$:$0.08Yb^{3+}$, $0.08Er^{3+}$, (c) $NaBi(MoO_4)_2$:$0.10Yb^{3+}$, $0.08Er^{3+}$, (d) $NaBi(MoO_4)_2$:$0.125Yb^{3+}$, $0.08Er^{3+}$, (e) $NaBi(MoO_4)_2$:$0.15Yb^{3+}$, $0.08Er^{3+}$, and (f) $NaBi(MoO_4)_2$:$0.175Yb^{3+}$, $0.08Er^{3+}$.

Table S1. Refined structural parameters of $NaBi(MoO_4)_2$: Yb^{3+}, Ho^{3+} nanomaterial.

Composition	**$NaBiMo_2O_8$**	**$NaBi_{0.98}Yb_{0.01}Ho_{0.01}Mo_2O_8$**	**$NaBi_{0.965}Yb_{0.025}Ho_{0.01}Mo_2O_8$**	**$NaBi_{0.94}Yb_{0.05}Ho_{0.01}Mo_2O_8$**	**$NaBi_{0.915}Yb_{0.075}Ho_{0.01}Mo_2O_8$**
Lattice	Tetragonal	Tetragonal	Tetragonal	Tetragonal	Tetragonal
Space Group	$I4_1/a$	$I4_1/a$	$I4_1/a$	$I4_1/a$	$I4_1/a$
a (Å)	5.2844(2)	5.2812(1)	5.2782(1)	5.2783(2)	5.2774(1)
c (Å)	11.5867(5)	11.5663(3)	11.5582(4)	11.5576(5)	11.5514(4)
V (Å^3)	323.55(2)	322.60(1)	322.01(1)	322.01(2)	321.71(1)
R_p	6.53	6.21	6.34	6.55	6.14
R_{wp}	8.47	8.23	8.24	8.08	8.24
χ^2	2.96	2.82	2.91	4.63	2.87
R_B	2.42	1.87	1.68	1.91	1.56
GOF	1.56	1.37	1.30	1.38	1.25

Table S2. Refined structural parameters of $NaBi(MoO_4)_2$: Yb^{3+}, $0.08Er^{3+}$ nanomaterial.

Composition	**$NaBi_{0.92}Er_{0.08}Mo_2O_8$**	**$NaBi_{0.84}Yb_{0.08}Er_{0.08}Mo_2O_8$**	**$NaBi_{0.82}Yb_{0.1}Er_{0.08}Mo_2O_8$**	**$NaBi_{0.795}Yb_{0.125}Er_{0.08}Mo_2O_8$**	**$NaBi_{0.77}Yb_{0.15}Er_{0.08}Mo_2O_8$**	**$NaBi_{0.745}Yb_{0.175}Er_{0.08}Mo_2O_8$**
Lattice	Tetragonal	Tetragonal	Tetragonal	Tetragonal	Tetragonal	Tetragonal
Space Group	$I4_1/a$	$I4_1/a$	$I4_1/a$	$I4_1/a$	$I4_1/a$	$I4_1/a$
a (Å)	5.2822(2)	5.2807(1)	5.2729(1)	5.2743(1)	5.2748(1)	5.2702(1)
c (Å)	11.5674(5)	11.5484(4)	11.5240(4)	11.5268(4)	11.5237(4)	11.5135(4)
V ($Å^3$)	322.75(2)	322.04(2)	320.41(1)	320.66(2)	320.64(2)	319.79(2)
R_p	6.98	7.30	6.52	6.58	6.14	6.37
R_{wp}	9.30	9.39	8.56	8.78	8.26	8.28
χ^2	4.41	4.20	3.27	3.15	3.19	2.95
R_B	2.52	2.15	2.01	2.49	1.68	2.01
GOF	1.59	1.47	1.42	1.58	1.30	1.42

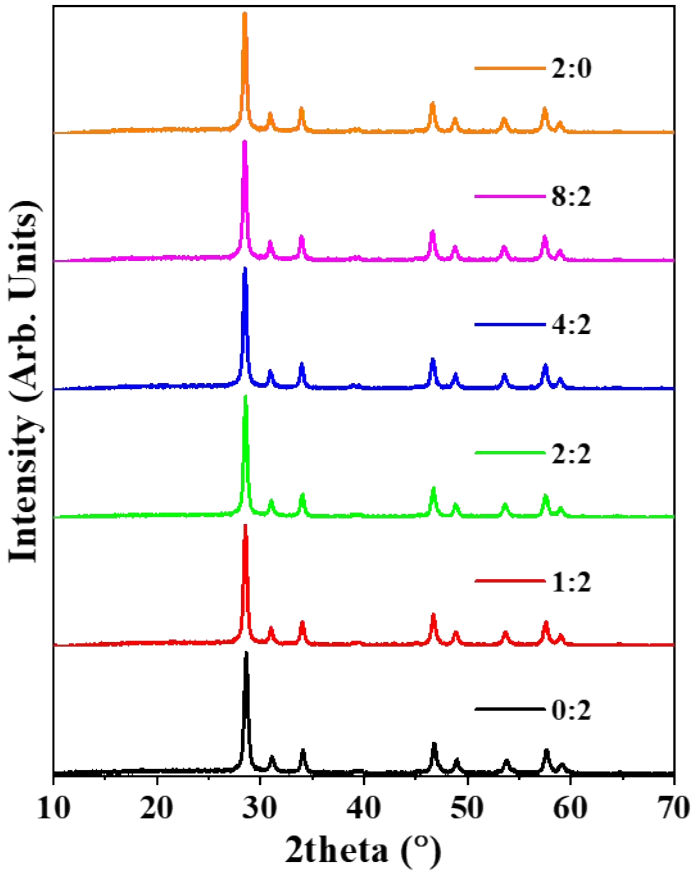

Fig. S4. XRD patterns of NBM: 0.15Yb^{3+}, 0.08Er^{3+}@ NBM: 0.05Yb^{3+}, 0.01Ho^{3+} core@shell series.

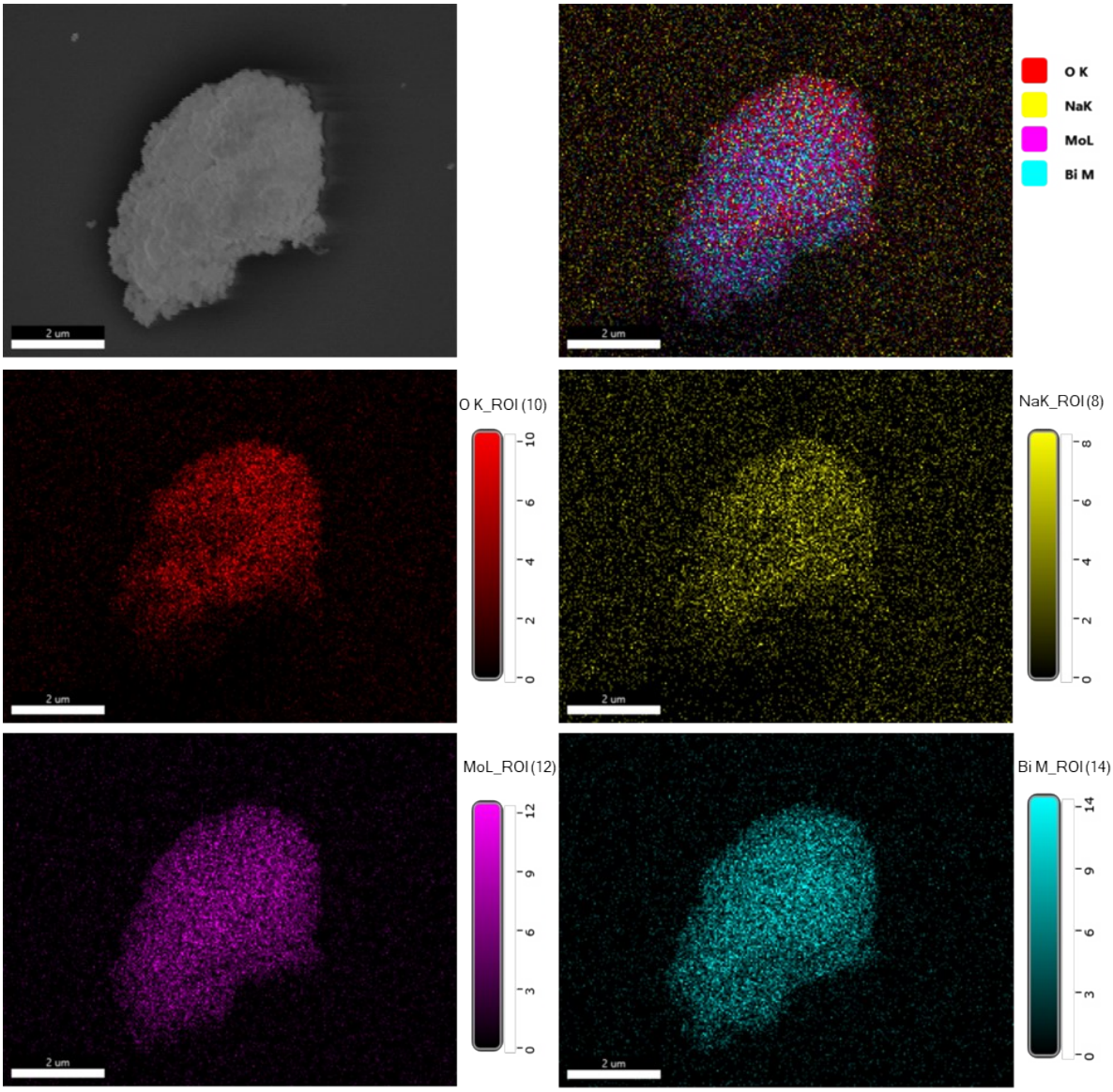

Fig. S5. Elemental Mapping of undoped $NaBi(MoO_4)_2$ nanoparticles.

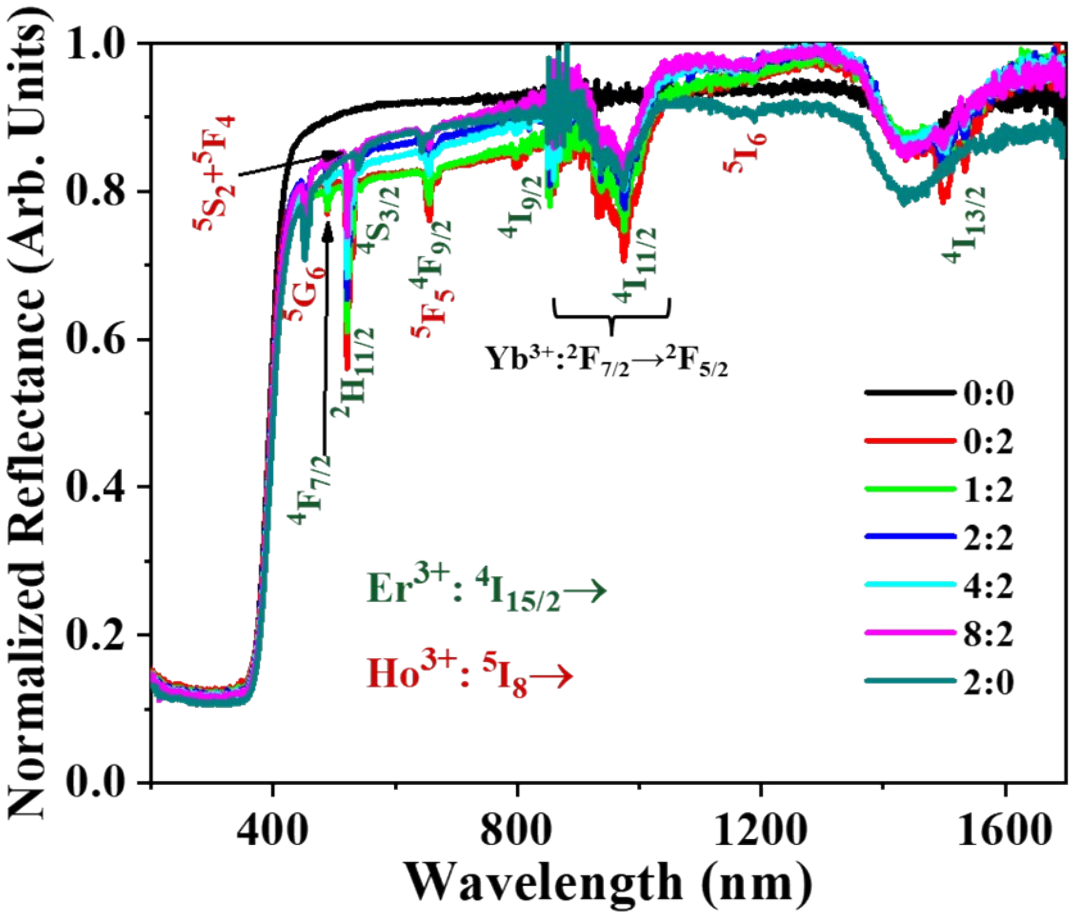

Fig. S6. UV-Visible-NIR diffuse reflectance spectra of NBM: 0.15Yb^{3+}, 0.08Er^{3+}@ NBM: 0.05Yb^{3+}, 0.01Ho^{3+} core@shell nanoparticles with different shell-to-core ratios. (0:0 is the only host material)

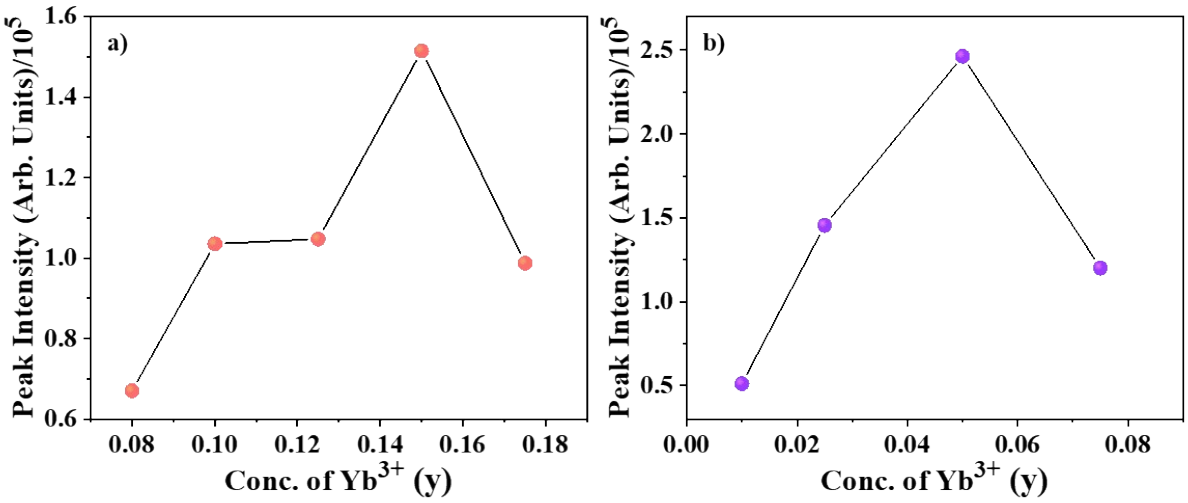

Fig. S7. UC emission intensity of (a) Yb^{3+}/Er^{3+} and (b) Yb^{3+}/Ho^{3+} codoped NBM as a function of concentration of Yb^{3+} ions.

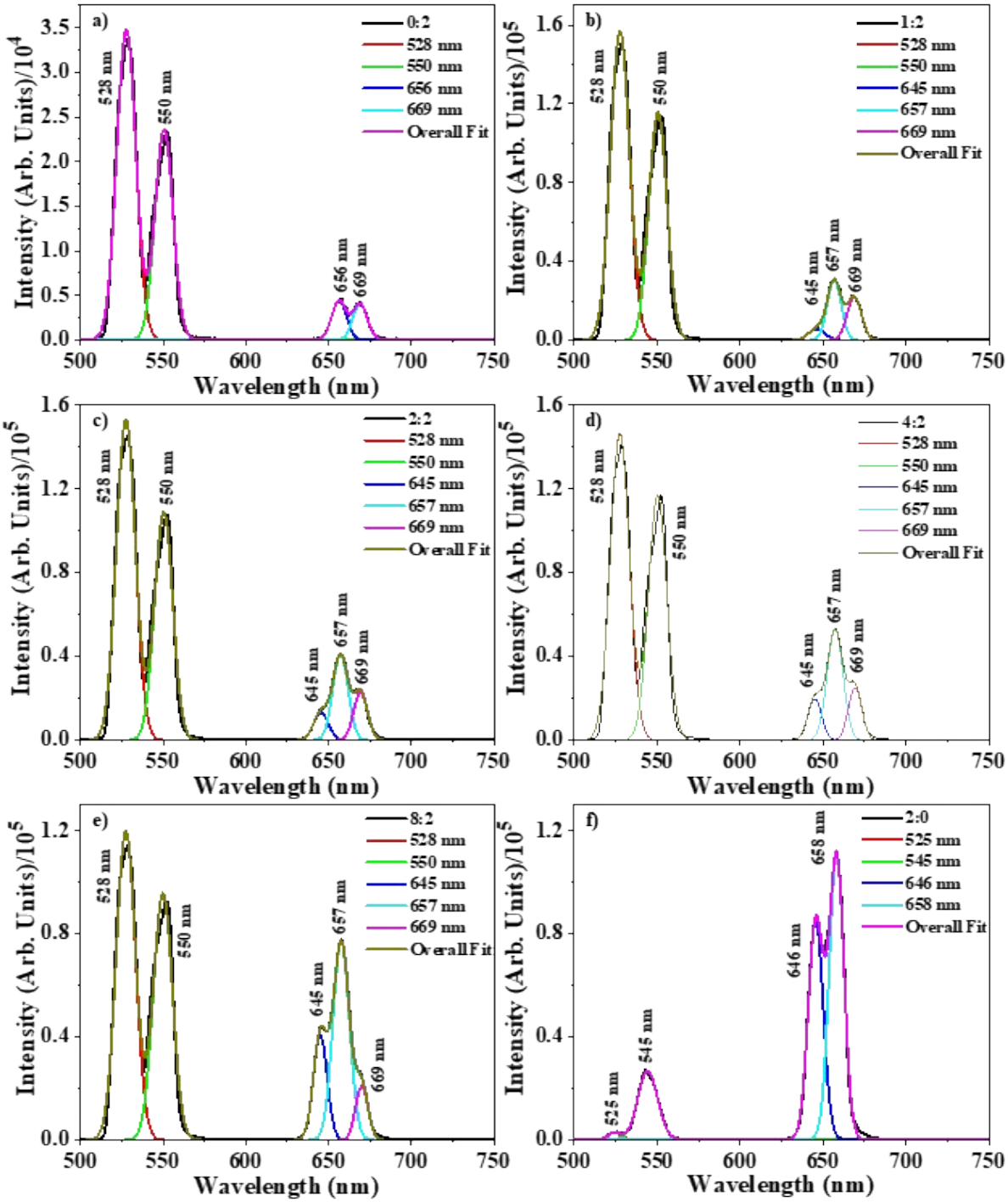

Fig. S8. Gaussian deconvoluted UC emission spectra of NBM: 0.15Yb^{3+}, 0.08Er^{3+}@ NBM: 0.05Yb^{3+}, 0.01Ho^{3+} core@shell series with varying shell-to-core ratios.

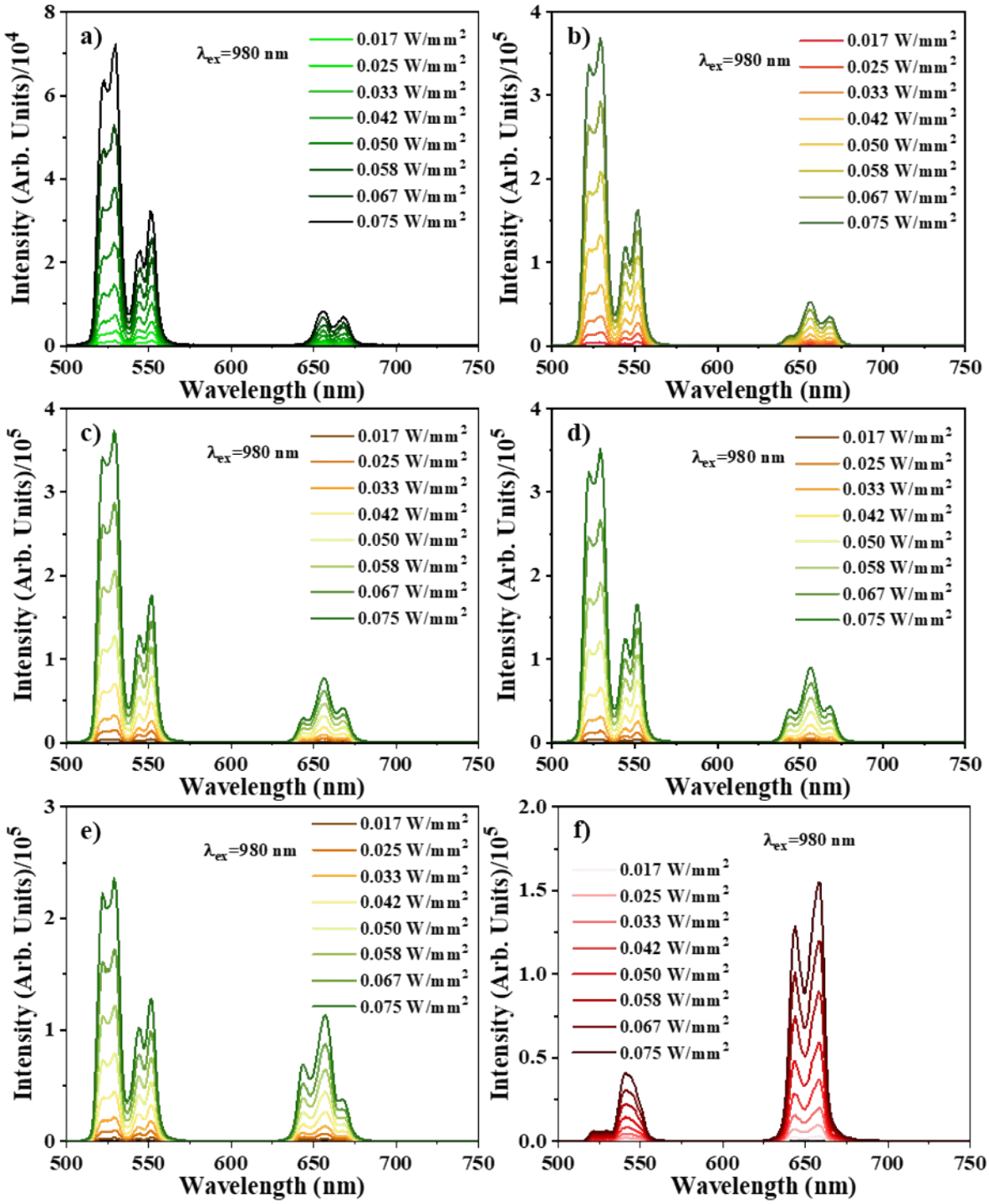

Fig. S9. UC luminescence spectra of NBM: 0.15Yb^{3+}, 0.08Er^{3+}@ NBM: 0.05Yb^{3+}, 0.01Ho^{3+} core@shell series with shell-to-core ratio **(a)** 0:2, **(b)** 1:2, **(c)** 2:2, **(d)** 4:2, **(e)** 8:2 and **(f)** 2:0 under various pump power.

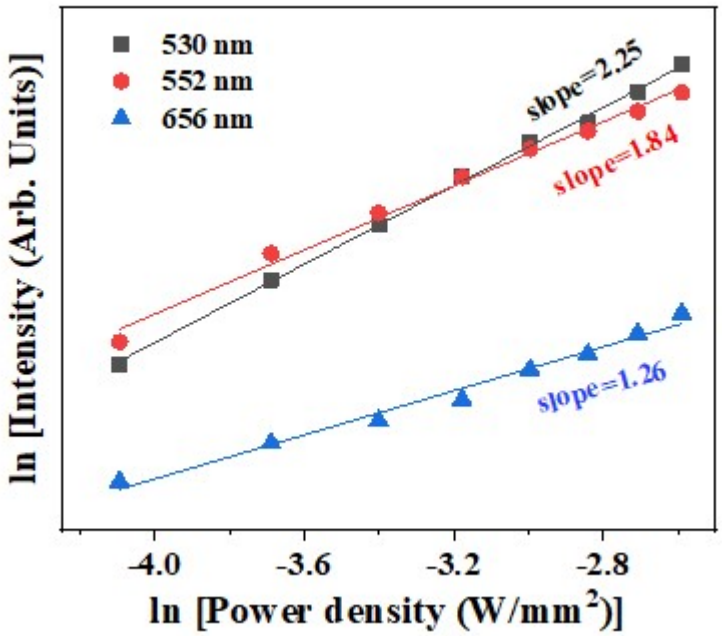

Fig. S10. Logarithmic variation of Intensity as a function of pump power of NBM: $0.08Er^{3+}$

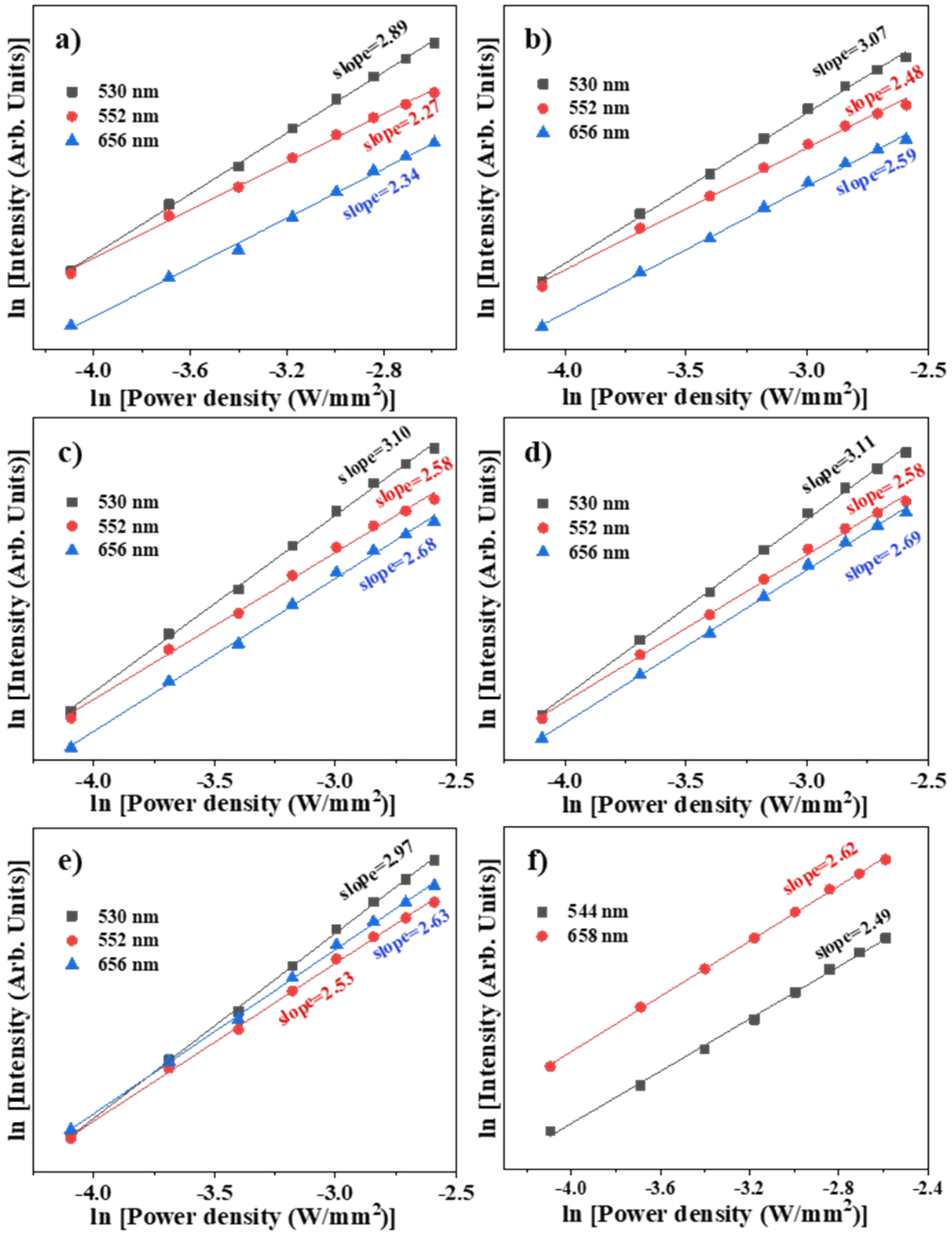

Fig. S11. Logarithmic variation of Intensity of NBM: 0.15Yb^{3+}, 0.08Er^{3+}@ NBM: 0.05Yb^{3+}, 0.01Ho^{3+} core@shell series with the shell-to-core ratio **(a)** 0:2, **(b)** 1:2, **(c)** 2:2, **(d)** 4:2, **(e)** 8:2 and **(f)** 2:0 with pump power density.

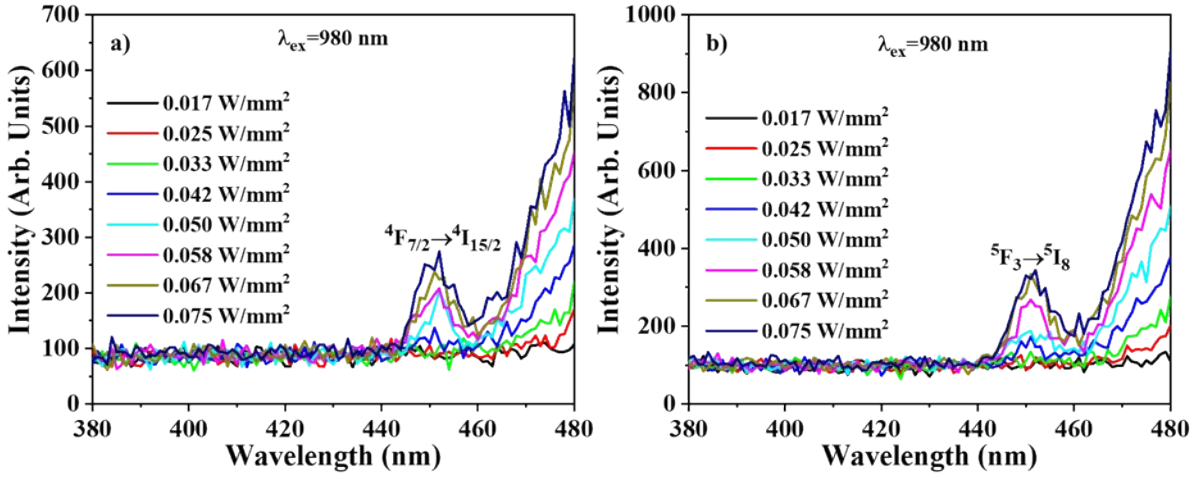

Fig. S12. UC emission spectra of (a) NBM:0.15 Yb^{3+}, 0.08 Er^{3+}, and (b) NBM:0.05 Yb^{3+}, 0.01 Ho^{3+} in the range of 380-480 nm.

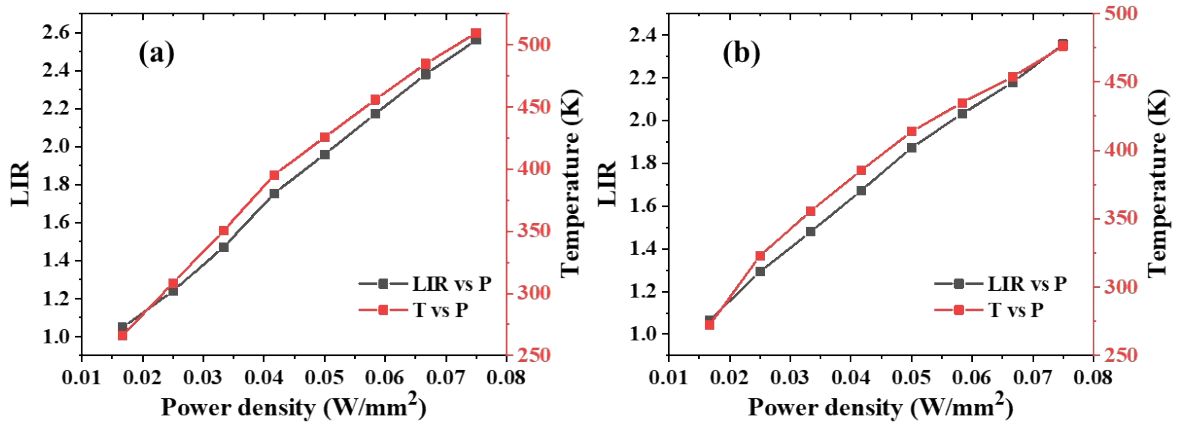

Fig. S13. Laser heating effect of pump power density in (a) NBM: 0.15Yb^{3+}, 0.08Er^{3+} and (b) core-shell nanoparticles showing the highest temperature sensitivity, i.e., NBM: 0.15Yb^{3+}, 0.08Er^{3+}@ NBM: 0.05Yb^{3+}, 0.01Ho^{3+} with the shell-to-core ratio of 4:2.

The enhancement in the slope value of the logarithmic variation of UC emission intensity with pump power density can be explained via the 'laser heating effect'. The two-photon upconversion process of Er^{3+} ions is well-known. On the other hand, we have identified it as a three-photon process based on the slope values we got for the 528 nm and 552 nm emission bands, which are more than 2.8 and 2.2, respectively, in the double-log plot of the power dependence of UC intensity. In this case, low and high powers make up the power variation. The intensity of the $^4S_{3/2}\rightarrow{}^4I_{15/2}$ transition becomes much lower, in contrast to the $^2H_{11/2}\rightarrow{}^4I_{15/2}$ transition, as the power density increases, which was almost identical at lower pump power (as shown in Figure S9 of the ESI). As the stimulation power was raised, the intensity ratio of the green emission bands, which showed a variance in intensity, rose. The LIR method states that the intensity ratio varies with temperature changes, and since the intensity ratio is dependent on pump power, it follows that temperature is connected to the excitation power of the pump. Crystalline powders absorbing energy and transferring it into heat through nonradiative pathways is the main cause of the power dependency temperature rise of the sample. [1] This optical heat generated by the laser can be calculated by rearranging Eq. (3) of the main manuscript to obtain:

$$T = \left(\frac{\Delta E}{k_B}\right) \times \left(\frac{1}{\ln B - \ln\left(LIR - C\right)}\right) \tag{E1}$$

Fig. S13a shows the results of the laser heating of the NBM:0.15 Yb^{3+}, 0.08 Er^{3+}. The LIR measurements showed a constant rise as the power increased. According to the characteristics of optical temperature sensing, a given value of LIR is correlated with a given temperature

value. According to Eq. (E1), the sample's temperature changes when exposed to laser stimulation at different power densities. As the power density increased from 0.017 to 0.075 W/mm^2, the temperature increased in a linear fashion. In light of the foregoing, UC emission materials may find use as optical heaters in photothermal treatment, because non-radiative relaxation (electron-phonon coupling) is critical for induced heat as power densities increase.

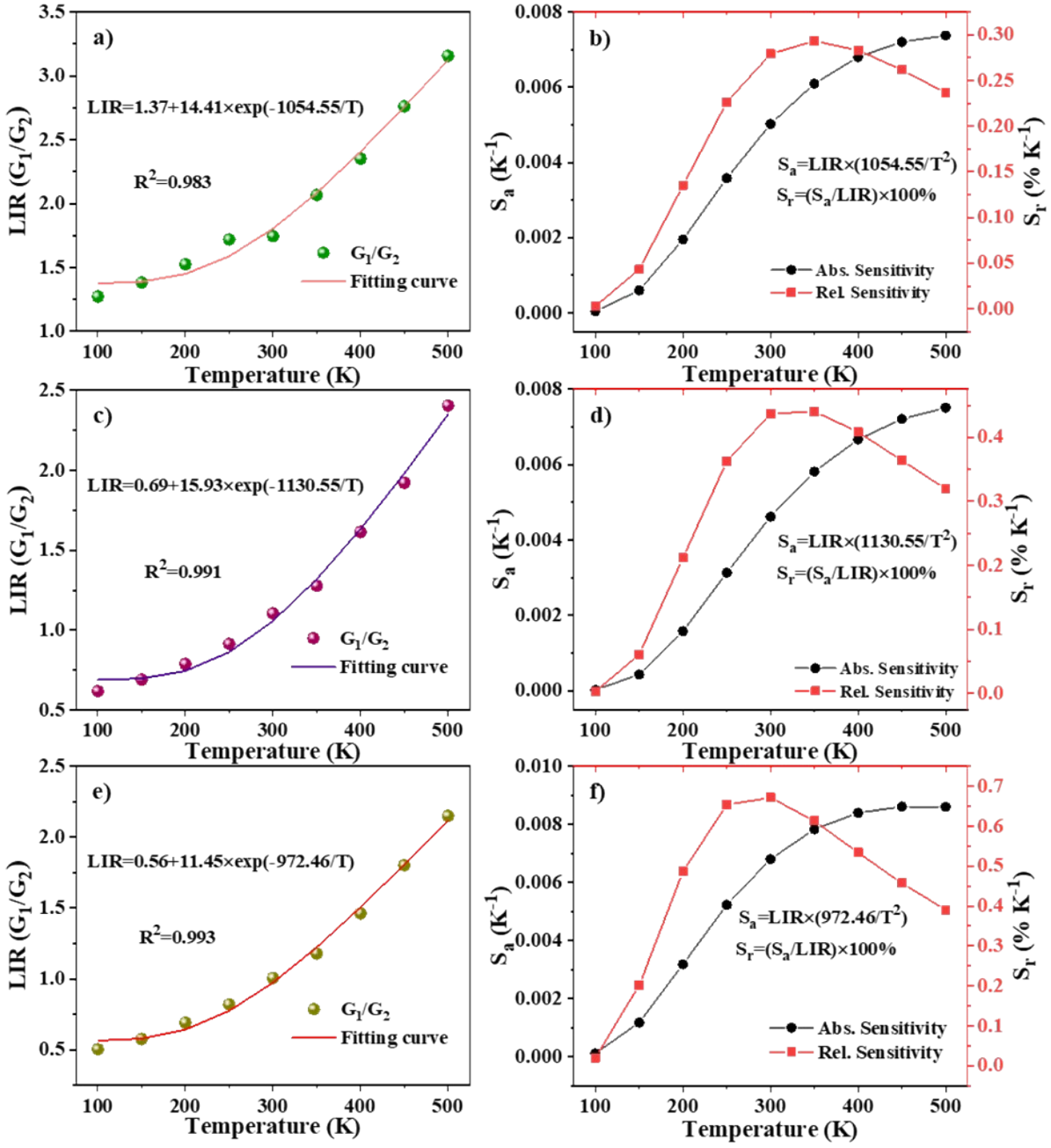

Fig. S14. LIR and the corresponding absolute and relative sensitivities for $\mathbf{G_1/G_2}$ TCELs of NBM: 0.15Yb^{3+}, 0.08Er^{3+}@ NBM: 0.05Yb^{3+}, 0.01Ho^{3+} core@shell series with the shell-to-core ratio of **(a, b)** 1:2, **(c, d)** 2:2, and **(e, f)** 8:2.

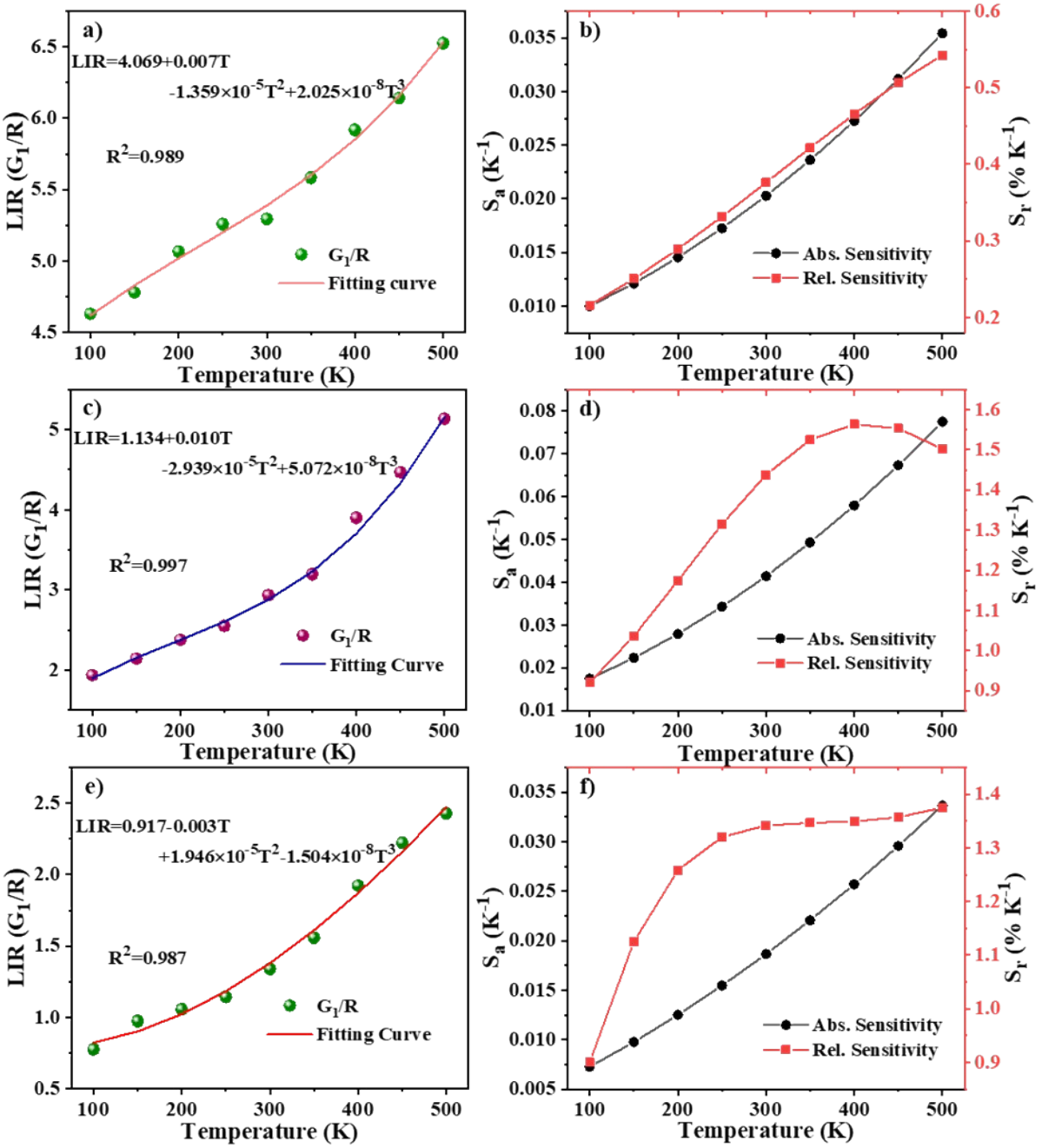

Fig. S15. LIR and the corresponding absolute and relative sensitivities for **G_1/R** NTCELs of NBM: 0.15Yb^{3+}, 0.08Er^{3+}@ NBM: 0.05Yb^{3+}, 0.01Ho^{3+} core@shell series with shell-to-core ratio of **(a, b)** 1:2, **(c, d)** 2:2, and **(e, f)** 8:2.

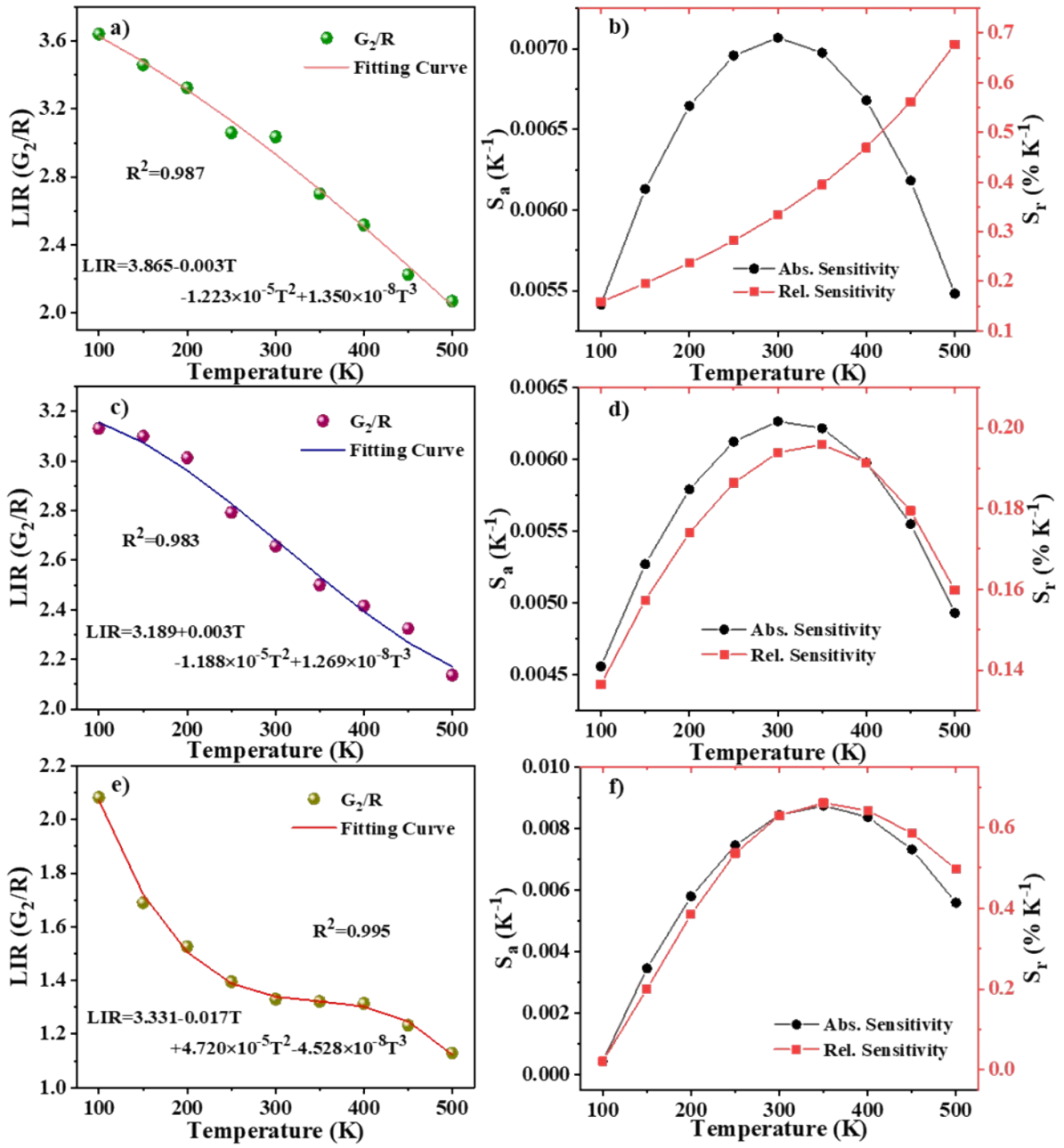

Fig. S16. LIR and the corresponding absolute and relative sensitivities for **G_2/R** NTCELs of NBM: 0.15Yb^{3+}, 0.08Er^{3+}@ NBM: 0.05Yb^{3+}, 0.01Ho^{3+} core@shell series with shell-to-core ratio of **(a, b)** 1:2, **(c, d)** 2:2, and **(e, f)** 8:2.

Table S3. Absolute and relative sensitivity values of NBM: 0.15Yb^{3+}, 0.08Er^{3+}@ NBM: 0.05Yb^{3+}, 0.01Ho^{3+} core@shell and NBM: 0.05Yb^{3+}, 0.08Er^{3+}, 0.01Ho^{3+} NPs optical thermometers.

NBM: 0.15Yb^{3+}, 0.08Er^{3+}@ NBM: 0.05Yb^{3+}, 0.01Ho^{3+} core@shell with shell-to-core ratio		**S_a (K^{-1})×10^{-4}**	**S_r (%.K^{-1})**
0:2	**G_1/G_2**	72.9	0.40
	G_1/R	220.1	0.28
	G_2/R	623.0	1.14
1:2	**G_1/G_2**	73.8	0.29
	G_1/R	354.3	0.54
	G_2/R	70.7	0.68
2:2	**G_1/G_2**	75.1	0.44
	G_1/R	775.1	1.56
	G_2/R	62.6	0.19
4:2	**G_1/G_2**	83.3	0.41
	G_1/R	1904.4	4.16
	G_2/R	76.2	0.35
8:2	**G_1/G_2**	86.1	0.67
	G_1/R	336.5	1.37
	G_2/R	330.4	2.66
2:0	**G_1/G_2**	1.3	0.15
	G_1/R	6.3	1.68
	G_2/R	6.2	0.02
NBM: 0.05Yb^{3+}, 0.08Er^{3+}, 0.01Ho^{3+} NPs	**G_1/G_2**	74.4	0.37
	G_1/R	1734.2	3.81
	G_2/R	42.7	0.14

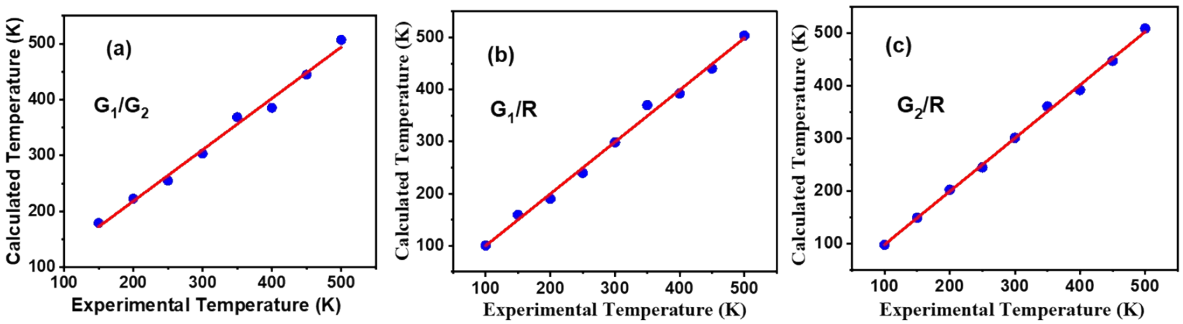

Fig. S17. Calibration curves for (a) G_1/G_2 TCELs, (b) G_1/R and (c) G_2/R NTCELs for highly sensitive sample, i.e., NBM: $0.15Yb^{3+}$, $0.08Er^{3+}$@ NBM: $0.05Yb^{3+}$, $0.01Ho^{3+}$ core@shell sample with shell-to-core ratio of 4:2. Measurements were carried out at pump power density of $0.042W/mm^2$.

Table S4. Temperature uncertainty values of NBM: 0.15Yb^{3+}, 0.08Er^{3+}@ NBM: 0.05Yb^{3+}, 0.01Ho^{3+} core@shell optical thermometers at 300 K.

Ratio	**G_1/G_2**	**G_1/R**	**R/G_2**
0:2	0.0043 K	0.0084 K	0.0085 K
1:2	0.0049 K	0.0075 K	0.0079 K
2:2	0.0053 K	0.0072 K	0.0073 K
4:2	0.0031 K	0.0059 K	0.0016 K
8:2	0.0029 K	0.0015 K	0.11 K
2:0	0.0157 K	0.0129 K	0.0159 K

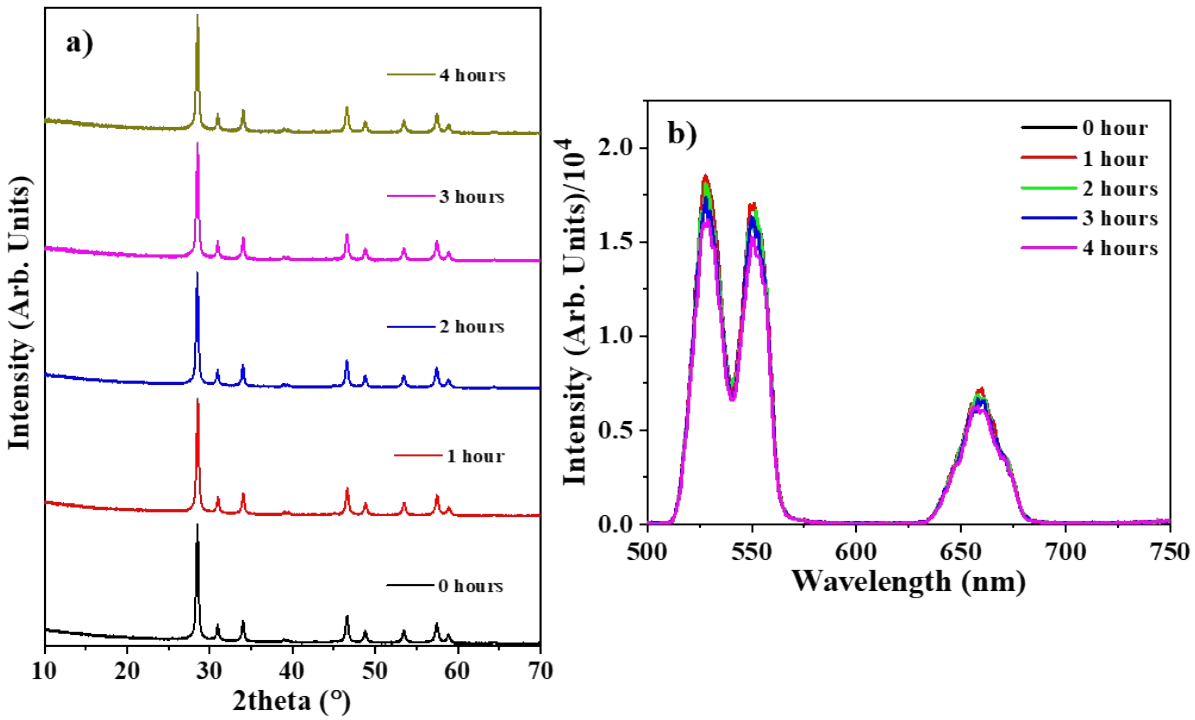

Fig. S18. (a) PXRD, and (b) PL intensity of NBM: 0.15Yb^{3+}, 0.08Er^{3+}@ NBM: 0.05Yb^{3+}, 0.01Ho^{3+} core@shell nanoparticles with 4:2 shell:core ratio under 'double 85' test.

References:

1 R. Dey, A. Pandey and V. K. Rai, *Sens Actuators B Chem*, 2014, **190**, 512–515.